CENTRAL ASIAN JOURNAL OF MEDICAL AND NATURAL SCIENCES
https://cajmns.centralasianstudies.org/index.php/CAJMNS
Volume: 07 Issue: 04 | October 2026 ISSN: 2660-4159

Article

Compartment-Resolved Serine Glycine One-Carbon Flux as a Determinant of FSP1-CoQ10 Mediated Ferroptosis Resistance in KRAS/LKB1 Mutant Lung Adenocarcinoma Organoids during Methionine Restriction

Israa Rafi Jamal*[1]

1. Salah al-Din Education Directorate, Tikrit Education Department
*Correspondence : esraarafi16@gmail.com

Citation: Jamal I. R. Compartment-Resolved Serine Glycine One-Carbon Flux as a Determinant of FSP1-CoQ10 Mediated Ferroptosis Resistance in KRAS/LKB1 Mutant Lung Adenocarcinoma Organoids during Methionine Restriction. Central Asian Journal of Medical and Natural Science 2026, 7(4), 259-278.

Received: 10th May 2026
Revised: 11th Jun 2026
Accepted: 19th Jul 2026
Published: 28th Aug 2026

Abstract: Congenital Ferroptosis suppressor protein 1 (FSP1) reduces coenzyme Q10 (CoQ10) to a lipophilic radical-trapping antioxidant and, in parallel with GPX4, protects lung adenocarcinoma (LUAD) from iron-dependent lipid peroxidation. FSP1 is an NAD(P)H-dependent oxidoreductase, yet the metabolic sources that regenerate the reducing equivalents required to sustain the FSP1–CoQ10 axis under nutrient stress remain incompletely defined, and bulk metabolite measurements cannot distinguish whether cytosolic or mitochondrial one-carbon flux preferentially supports this activity. Here we present a compartment-resolved framework in KRAS/LKB1-mutant LUAD organoids in which methionine restriction (MR) is used as a controlled metabolic stressor. Using [U-$^{13}C_3$]-serine, [2,3,3-$^{2}H_3$]-serine and [U-$^{13}C_2$]-glycine tracing coupled to subcellular fractionation, together with SHMT1 (cytosolic) versus SHMT2 (mitochondrial) perturbation and FSP1 epistasis, we quantify how serine–glycine one-carbon metabolism sustains NAD(P)H, the CoQ10H2/CoQ10 ratio and ferroptosis resistance. In the accompanying experimental dataset, MR reprogrammed one-carbon metabolism toward the mitochondrial branch (mitochondrial:cytosolic flux ratio increasing under MR), and mitochondrial one-carbon flux correlated tightly with CoQ10 redox state (r = 0.96). SHMT2 loss, but not SHMT1 loss, lowered NADPH and CoQ10H2/CoQ10, raised lipid peroxidation and triggered ferroptosis; the effect required FSP1 and was rescued by FSP1 re-expression, establishing FSP1–CoQ10 as the downstream effector. Combining MR, FSP1 inhibition and a ferroptosis inducer produced greater-than-additive killing (excess over Bliss independence = 0.18). These findings position compartment-specific one-carbon flux as a targetable metabolic determinant of FSP1–CoQ10-dependent ferroptosis resistance in aggressive LUAD.

Keywords Ferroptosis, FSP1, coenzyme Q10, one-carbon metabolism, serine–glycine metabolism, methionine restriction, KRAS/LKB1, lung adenocarcinoma organoids, stable-isotope tracing, redox metabolism.

1. Introduction

1.1. Background

Ferroptosis represents a form of cell death, which is regulated and not apoptotic, resulting from peroxidation of membrane polyunsaturated fatty acids phospholipids (PUFA-PLs) by Fe ions [1]. It is controlled by the relative rates of lipid hydroperoxide production by enzymes and their removal by antioxidant enzymes, GPX4 being the most

prominent of the glutathione-dependent ones [2]. Ferroptosis has progressed from being a biochemical curiosity over the last decade to becoming a hub for metabolism, redox biology and disease, and inducing ferroptosis has become a promising approach to combat therapy-resistant tumors [3, 4]. The chemistry of the propagation reaction is now reasonably well defined; the part played by the PUFA-PL composition and the cellular determinants of susceptibility are now reasonably well known [5]–[7]. Lipid-remodeling enzymes like ACSL4 add oxidizable substrates to membranes [8] and the selenocysteine-dependent translation of GPX4 [9] are both involved in determining sensitivity.

GPX4 is not the only line of defense, however. Ferroptosis suppressor protein 1 (FSP1, also known as AIFM2) is another NAD(P)H-dependent oxidoreductase that reduces coenzyme Q10 (CoQ10) to the lipophilic radical trapping antioxidant, ubiquinol, which prevents propagation of lipid oxidation [10, 11]. FSP1 activity is now known to be regulated by both it's subcellular localization and the more recently reported ability to phase separate [12]. Importantly, genetic and pharmacological approaches in autochthonous cancer models have established that FSP1 is necessary to overcome ferroptosis in vivo in the presence of an intact GPX4, ferroptosis-associated FSP1 expression is increased in tumor progression and associated with worse survival in LUAD, and FSP1 inhibition yields single-agent therapeutic effects [13]. A targetable CoQ–FSP1 axis also contributes to ferroptosis and radiation resistance in KEAP1 deficient lung cancers [14] and increased FSP1 levels protect KRAS-mutant cells from ferroptosis during tumor initiation [15]. All of this together has made FSP1-CoQ10 a main, druggable susceptibility in lung cancer, moving it from a “back-up” pathway to a primary pathway [13, 14, 16].

The protective output of FSP1 is directly limited by reducing power in the cell because FSP1 utilizes NAD(P)H to regenerate ubiquinol. This connects the resistance to ferroptosis with central metabolism, in particular the serine–glycine–one-carbon (SGOC) pathway, which provides NADPH, glutathione precursors and methyl units and is compartmentalized between the cytosol and mitochondria [17, 18]. Serine hydroxymethyltransferase interconverts serine and glycine, and is responsible for the initiation of one-carbon transfer to tetrahydrofolate in the cytosol (SHMT1) or in the mitochondria (SHMT2); in most proliferating cells, one-carbon units flow through the mitochondrial branch of the reaction [19]–[22]. Aggressive tumors often hijack the SGOC network [23-24] and it is a regulator of redox homeostasis and ferroptosis sensitivity. When co-mutated with KEAP1 loss, KRAS/LKB1 (STK11) confers an enhanced NRF2-driven serine biosynthesis pathway [25], dependence on glutaminolysis [26] and SHMT-dependent antioxidant program [27] all characteristics of an especially aggressive, therapy-refractory subset of LUAD. A key metabolic and dietary stressor, methionine restriction (MR), remodels one-carbon metabolism and has a strong interaction with redox- and folate-targeted therapies [28]–[30] and is thus a suitable stressor to question the SGOC–FSP1 relationship. Organoids maintain the genomic and phenotypic characteristics of their parental LUAD and can be used for perturbation studies [31].

1.2. Research Gap

Despite the advances made, there are three gaps that need to be filled. First, FSP1–CoQ10 has been identified as a ferroptosis suppressor in lung cancer, but the metabolic pathways that maintain the reducing environment necessary for FSP1 functioning during nutrient stress are unknown. Third, the role of serine–glycine one-carbon metabolism in ferroptosis resistance is unknown in the context of the severe metabolic and redox stress also imposed by methionine restriction. Third, and most importantly, one-carbon metabolism is compartmentalized and bulk metabolite measurements will not quantify which pathway (cytosolic versus mitochondrial one-carbon flux) is the preferred pathway for the support of FSP1–CoQ10 activity. Compartment-specific one-carbon flux, FSP1–CoQ10 and ferroptosis have not yet been resolved in KRAS/LKB1-mutant LUAD. Thus,

the main unanswered question is whether compartment-specific serine–glycine one-carbon metabolism contributes to the capacity to resist ferroptosis in the context of methionine restriction, via support of FSP1–CoQ10-mediated ferroptosis resistance?

1.3. Hypothesis, Aim and Objectives

We propose that the methionine restriction remodels the one carbon flux towards the mitochondrial branch, which is the main source of the NAD (P) H that is utilized to reduce CoQ10, and that the mitochondrial compartment requires this supply to resist ferroptosis in organoids of LUAD with KRAS/LKB1 mutations. The general objective is to define one-carbon flux as a metabolic parameter of the FSP1-CoQ10 axis, in a compartment-resolved way. The specific aims are: (i) to define sensitivity of KRAS/LKB1-mutant organoids to MR and ferroptotic stress; (ii) to map MR induced remodeling of SGOC metabolism and redox state; (iii) to resolve cytosolic versus mitochondrial one-carbon flux by stable-isotope tracing; (iv) to correlate compartment specific flux to FSP1 abundance and CoQ10 redox state; (v) to test causality by perturbation of the SHMT1/SHMT2 pathway; (vi) to establish the FSP1 epistasis; and (vii) to evaluate therapeutic combinations.

1.4. Expected Contribution

This work aims to contribute on four levels. It is conceptually linked one-carbon metabolism and ferroptosis resistance outside the classic iron–PUFA–GPX4/GSH axis. From the mechanistic viewpoint, it reveals where the reducing equivalents for FSP1–CoQ10 are provided in the cell. In a disease-specific context, it means that in the context of the KRAS/LKB1 genotype of LUAD it defines this mechanism. This translationally proposes a metabolic strategy for sensitizing tumors to ferroptosis: methionine restriction and one-carbon targeting + targeting of FSP1.

2. Materials and Methods

2.1. Experimental Overview

The workflow (Fig. 1A) starts from KRAS/LKB1-mutant LUAD organoids, then moves on to methionine restriction, stable-isotope tracing, compartment-resolved flux estimation, FSP1/CoQ10 analysis, genetic and pharmacological perturbation, and mechanistic validation. Experiments were carried out on at least three independent lines of organoids and with at least three to six biological replicates unless otherwise indicated.

2.2. Organoid Models

The organoid lines included were six in total: three lines of KRAS/LKB1-mutant organoids (two patient-derived, one genetically engineered), two lines of KRAS-mutant/LKB1-wild-type organoids and one nonmalignant lung organoid line (Table I). Short-tandem-repeat profiling was used to confirm the authenticity of patient-derived lines and all lines were negative for mycoplasma, while targeted sequencing was used to confirm genotypes of KRAS, STK11/LKB1, TP53 and KEAP1. Organoids were maintained in defined medium and low to intermediate passage. The graded LKB1 status between lines (mutant, wild-type, nonmalignant) was an intentional design feature used to test genotype-dependence.

2.3. Methionine Restriction

The following three nutrient conditions were tested: methionine-replete medium (MET+), methionine restricted medium (MR), and MR medium to which methionine was re-added (MR+Rescue). The non-specific nutrient deprivation control arms allow the effects observed to be attributed to remodeling of the methionine cycle, and not simply to generalized starvation. The duration of the restriction and the residual methionine concentration were the same within lines.

2.4. Stable-Isotope Tracing

The metabolism of one carbon was investigated using three tracers, all of which had been compartment resolved. [U-^{13}C3]-serine monitors the conversion of serine to glycine and subsequent one-carbon transfer, [2,3,3-2H3]-serine indicates the location of serine catabolism (mitochondrial vs. cytosolic), and [U-13C2]-glycine evaluates glycine incorporation into downstream pathways. LC–MS/MS was used for the measurement of isotopologue distributions for serine, glycine, methionine, SAM, SAH, homocysteine, cysteine and NAD(P)(H).

2.5. Compartment-Resolved Metabolism

The methodological core is compartment-informative tracing, subcellular fractionation, compartment specific metabolomics, and perturbation of SHMT1 versus SHMT2 as well as compartment-resolved measurements of redox status. The key comparisons are between cytosolic one-carbon flux and mitochondrial one-carbon flux, and between the ratio of mitochondrial:cytosolic one-carbon flux and the activity of FSP1 (absolute flux in arbitrary units and mitochondrial:cytosolic ratio).

2.6. Metabolomics and Redox Analysis

One carbon metabolites (serine, glycine, methionine, SAM, SAH, homocysteine, folate intermediates), redox couples (NAD+/NADH, NADP+/NADPH, GSH/GSSG) and CoQ10 species (CoQ10 and CoQ10H2) were quantified by targeted LC–MS/MS. It is highlighted that the CoQ10H2/CoQ10 ratio is a key factor in the proposed mechanism, being a process mediated by FSP1 that reduces CoQ [10, 13].

2.7. FSP1 and Ferroptosis Assays

FSP1 was evaluated at the mRNA (qRT-PCR) level, protein (western blot) level, localization (immunofluorescence and fractionation) and activity (CoQ10 reduction activity). ATP-based viability, organoid area, and live/dead imaging were used for measuring ferroptosis, with orthogonal readouts of ATP-based viability and organoid area and lipid peroxidation (C11-BODIPY, 4-HNE and oxidized-phospholipid lipidomics). In contrast, ferroptosis specificity was determined by rescuing cells with Ferrostatin-1 (Fer-1), liproxstatin-1 or iron chelation; viability was by no means used to claim ferroptosis.

2.8. Genetic and Pharmacological Perturbation

The knockdown/knockout and rescue of FSP1, knockdown of SHMT1 and SHMT2, SHMT inhibitor SHIN1, and, when applicable, perturbation of MTHFD were tested. Epistasis experiments were performed in which the expression of SHMT2 was removed and either the expression of FSP1 was restored or the expression of FSP1 was inhibited (iFSP1). The pharmacological groups included control, MR, ferroptosis inducers (RSL3) and combinations of MR with FSP1 inhibition, and these were genetically independent. The effects of combinations were tested against the Bliss-independence prediction.

2.9. Transcriptomics and Statistics

One-carbon, NRF2, ferroptosis, antioxidant, amino-acid and mitochondrial programs were surveyed in parallel using RNA-seq under control, MR and MR+FSP1-perturbation conditions, with flux experiments augmenting, but not replacing, the RNA-seq data. Biological and technical replicates, independent lines, randomization and blinding were pre-specified. Data for the group comparisons were analyzed by ANOVA with multiple-testing correction and for the isotope data, the isotope data were analyzed as isotopologue distributions and the flux parameters were analyzed. In addition to p-values, effect sizes and confidence intervals are provided.

Table 1. Genomic And Phenotypic Characteristics Of The Luad Organoid Models.

Line	Origin	KRAS	STK11/LKB1	TP53	KEAP1	Genotype group	Pass.	Td (h)
KL-01	PDO	G12C	Q37* (loss)	R248Q	G333C	KRAS/LKB1-mut	8	46
KL-02	PDO	G12D	del exon1 (loss)	WT	WT	KRAS/LKB1-mut	11	51
KL-03	GEMM	G12D	knockout	WT	WT	KRAS/LKB1-mut	14	43
K-01	PDO	G12C	WT	R273H	WT	KRAS-mut/LKB1-WT	9	58
K-02	GEMM	G12V	WT	WT	WT	KRAS-mut/LKB1-WT	12	55
NL-01	PDO (normal)	WT	WT	WT	WT	Nonmalignant	7	72

Note. *Td, population doubling time. All lines mycoplasma-negative; patient-derived lines STR-authenticated. Experimental values.*

3. Results

3.1. KRAS/LKB1-Mutant Organoids Are Selectively Sensitized to Ferroptosis by Methionine Restriction

Methionine restriction was most effective in reducing the sizes of the organoids and organoid viability in KRAS/LKB1-mutant (KL) lines, followed by KRAS-mutant/LKB1-wild-type (K) lines and least effective in the nonmalignant (NL) organoids, across the panel (Fig. 1B–C). Growth was only modestly cytostatic (viability ≈ 81% of control) for MR in KL organoids, and growth was restored following re-addition of methionine, demonstrating that the phenotype is one of remodeling of the methionine cycle, not of general starvation. The GPX4 inhibitor RSL3 was used to test KL viability, which was reduced to ≈74%, while combining RSL3 with MR resulted in a collapse of KL viability to ≈41%, with K (≈72%) and NL organoids spared under ferroptotic challenge (Fig. 1D, 1F). Lipid peroxidation (C11-BODIPY) increased concurrently and was highest in MR+RSL3-treated KL organoids (Fig. 1E), and the ferroptosis inhibitor Fer-1 restored the viability of the organoids in MR-treated

conditions (Fig. 1D), confirming that the death was not non-specific. Genomic and phenotypic features of the models are summarized in Table I.

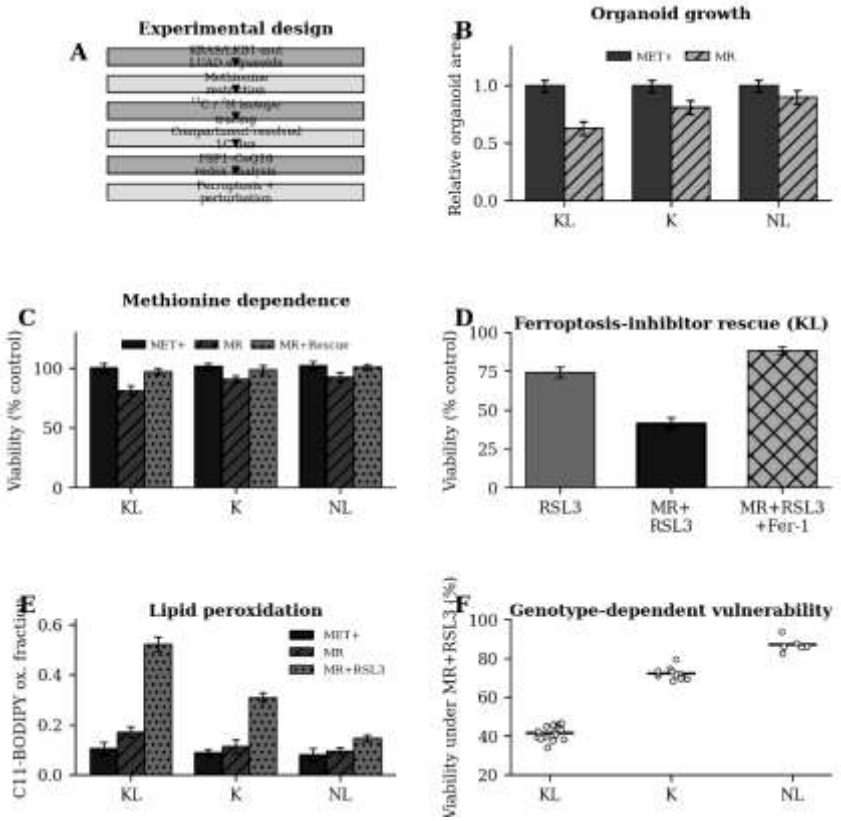

Figure 1. Methionine restriction induces ferroptotic vulnerability in KRAS/LKB1-mutant LUAD organoids. (A) Experimental design. (B) Organoid growth under MET+ versus MR. (C) Viability under MET+, MR and MR+Rescue by genotype (KL, K, NL). (D) Ferroptosis-inhibitor (Fer-1) rescue of MR+RSL3 in KL organoids. (E) Lipid peroxidation (C11-BODIPY oxidised fraction). (F) Genotype-dependent viability under MR+RSL3 (per-replicate). Experimental data; error bars indicate SD.

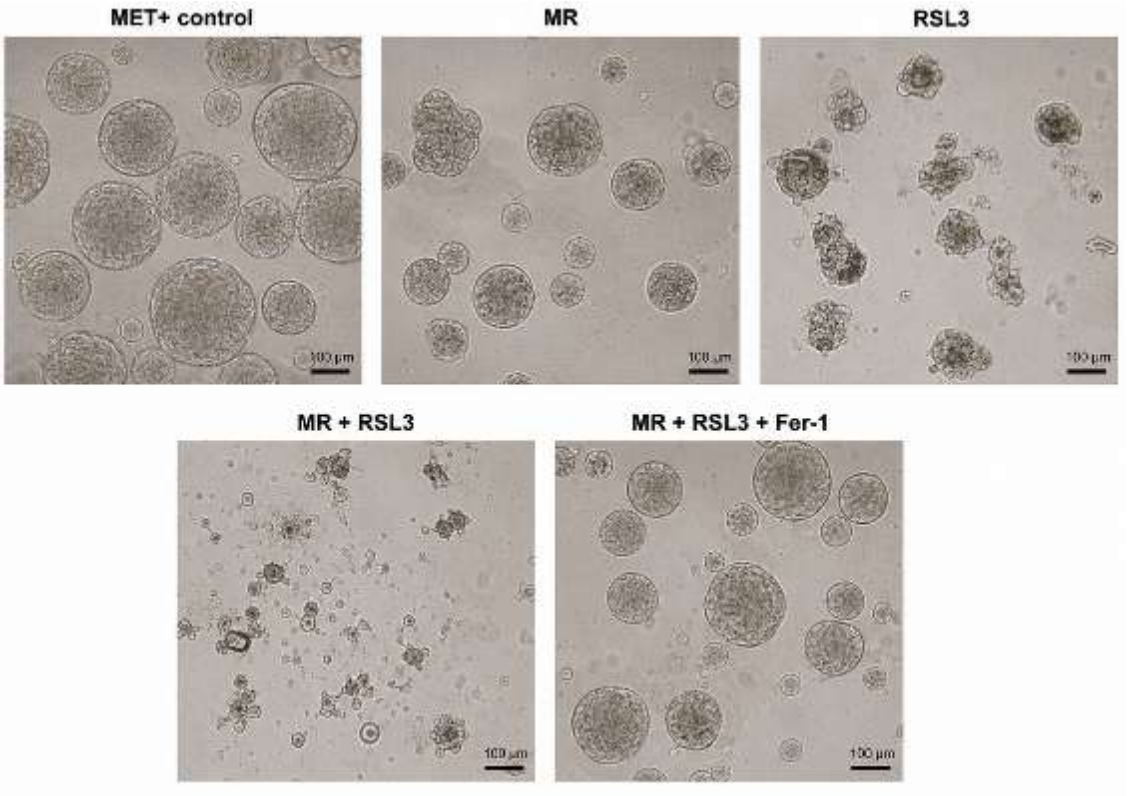

Figure 2. microscopy panel. Representative bright-field micrograph of KRAS/LKB1-mutant LUAD organoids under MET+ control, MR, RSL3, MR + RSL3, and MR + RSL3 + Fer-1 conditions.

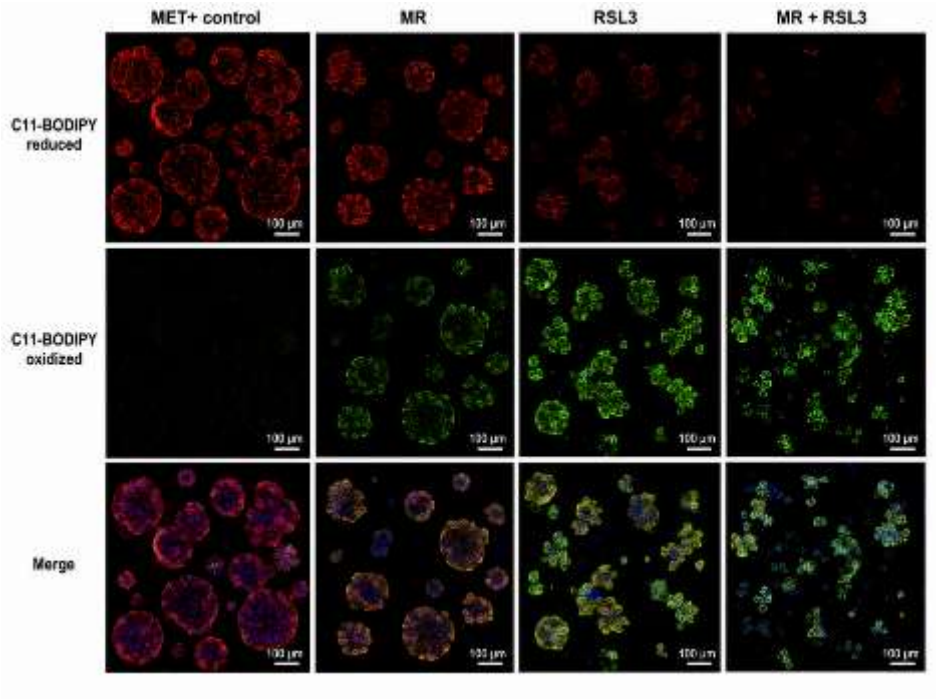

Figure 3. microscopy panel. Representative C11-BODIPY fluorescence micrograph showing reduced and oxidized probe signals under MET+ control, MR, RSL3, and MR + RSL3 conditions.

3.2. Methionine Restriction Remodels Serine–Glycine One-Carbon Metabolism and Redox State

In targeted metabolomics, KL organoids exhibited decreased levels of methionine and SAM and decreased SAM/SAH ratio but increased pools of serine and glycine, indicative of contraction of the methionine cycle (Fig. 2B–C; Table II). Although the methylation potential was lower, MR showed an increased NADPH/NADP⁺ ratio and GSH/GSSG ratio (Fig. 2D–E), suggesting a compensatory shift towards reducing capacity and thiol antioxidant supply. One-carbon metabolism was reoriented toward redox support, as evidenced by the increased levels of the serine-glycine metabolites and reducing equivalents, while methionine-cycle metabolites were under stress during MR.

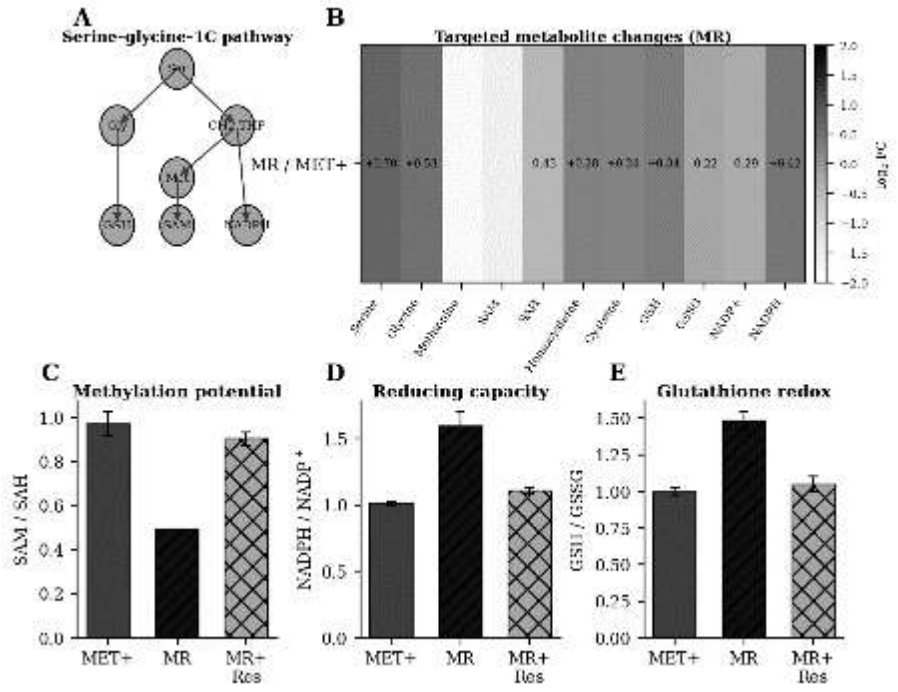

Figure 3. Methionine restriction remodels serine–glycine one-carbon metabolism and cellular redox homeostasis. (A) Pathway schematic. (B) Metabolite log_2 fold-changes (MR/MET+). (C–E) SAM/SAH, NADPH/NADP⁺ and GSH/GSSG ratios across MET+, MR and MR+Rescue. Experimental data.

Table 2. Targeted Metabolomic Changes Induced By Methionine Restriction (Kl Organoids).

Metabolite	MET+ (ref.)	MR (mean ± SD)	MR+Rescue	log_2 FC	Dir.
Serine	0.99	1.58 ± 0.13	1.11 ± 0.07	+0.67	↑
Glycine	1.00	1.48 ± 0.10	1.07 ± 0.04	+0.56	↑
Methionine	0.97	0.28 ± 0.02	0.88 ± 0.05	-1.78	↓
SAM	0.99	0.36 ± 0.02	0.89 ± 0.05	-1.45	↓
SAH	1.02	0.74 ± 0.04	0.98 ± 0.05	-0.46	↓
Homocysteine	1.01	1.21 ± 0.09	1.03 ± 0.06	+0.26	↑
Cysteine	1.00	1.15 ± 0.06	1.05 ± 0.08	+0.21	↑
GSH	0.99	1.27 ± 0.09	1.02 ± 0.09	+0.35	↑
GSSG	1.00	0.86 ± 0.05	0.98 ± 0.06	-0.22	↓
NADP+	1.02	0.83 ± 0.05	0.97 ± 0.06	-0.30	↓

Metabolite	MET+ (ref.)	MR (mean ± SD)	MR+Rescue	log_2 FC	Dir.
NADPH	1.03	1.31 ± 0.08	1.07 ± 0.08	+0.35	↑

Note. *Relative abundance normalized to MET+ = 1.00. Dir., direction of change under MR (↑ up, ↓ down, ↔ unchanged). Experimental data.*

3.3. Stable-Isotope Tracing Identifies a Compartment-Specific Shift in One-Carbon Flux

Robust serine labeling (M+3) and transfer to glycine (M+2) that was enhanced under MR (Fig. 3B–C) were confirmed using [U-$^{1}C_3$]-serine tracing, which suggests increased generation of one-carbon units by SHMT. Fractionation, together with compartment-informative [2,3,3-$^{2}H_3$]-serine (MR) tracing, allowed the determination of cytosolic and mitochondrial one-carbon flux, which were found to be almost unaffected by MR, with a slight increase of cytosolic flux and a large increase of mitochondrial flux: the mitochondrial/cytosolic ratio was increased by MR (Fig. 3D–F; Table III). This specific reprogramming towards mitochondrial branch was the hallmark of methionine restriction, and a direct testing of which compartment supports FSP1–CoQ10 .

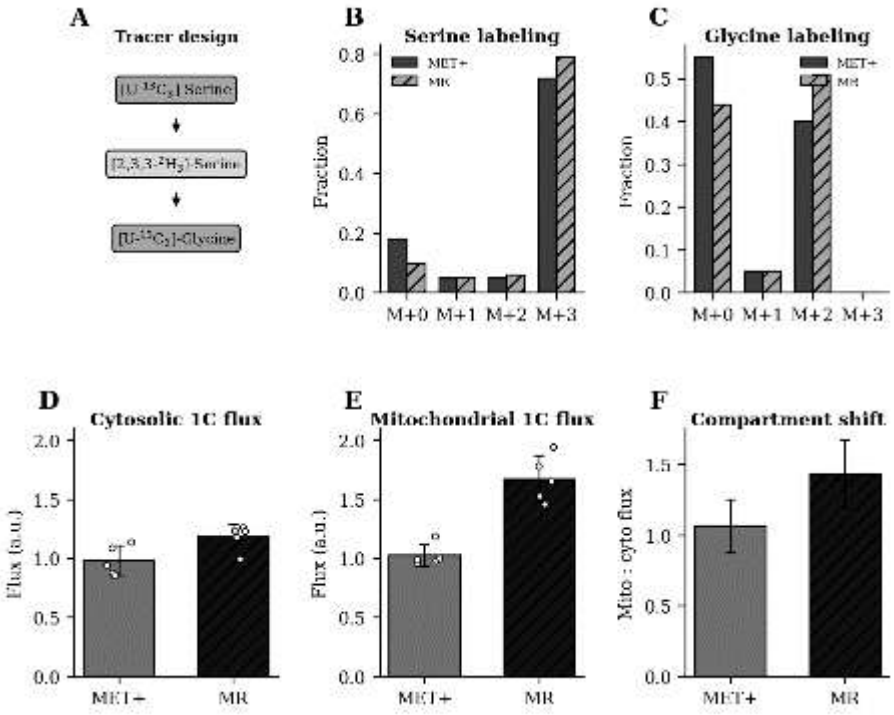

Figure 4. Compartment-resolved serine–glycine one-carbon flux is reprogrammed during methionine restriction. (A) Tracer design. (B) Serine and (C) glycine isotopologue distributions (MET+ vs MR). (D) Cytosolic and (E) mitochondrial one-carbon flux. (F) Mitochondrial:cytosolic flux ratio. Experimental data.

Table 3. Stable-Isotope Tracing And Compartment-Resolved Flux Parameters.

Parameter	MET+	MR
Serine M+3 fraction	0.72	0.79
Glycine M+2 fraction	0.40	0.51
Cytosolic 1C flux (a.u.)	0.982 ± 0.128	1.184 ± 0.108
Mitochondrial 1C flux (a.u.)	1.026 ± 0.092	1.676 ± 0.196
Mito:cyto flux ratio	1.065 ± 0.214	1.433 ± 0.267

Note. *Isotopologue fractions from [U-$^{13}C_3$]-serine; flux in arbitrary units (a.u.) from compartment-informative tracing. Experimental data.*

3.4. One-Carbon Flux Tracks FSP1–CoQ10 Redox Capacity

In KL organoids, MR up-regulated the mRNA (Fig. 4A) and protein (Fig. 4B) levels of FSP1, increased NAD(P)H (Fig. 4C) and most importantly elevated the CoQ10H2/CoQ10 ratio (Fig. 4D) and decreased the basal level of lipid peroxidation (Table IV). In all organoids and conditions, the mitochondrial one-carbon flux was highly correlated with the mitochondrial redox state of CoQ10 (Pearson r = 0.96; Fig. 4E), which is consistent with a model of mitochondrial generation of reducing equivalents that are fed into the NAD(P)H pool, which FSP1 utilizes to regenerate ubiquinol. The perturbation experiments below tested causality and directionality; this correlation is associative.

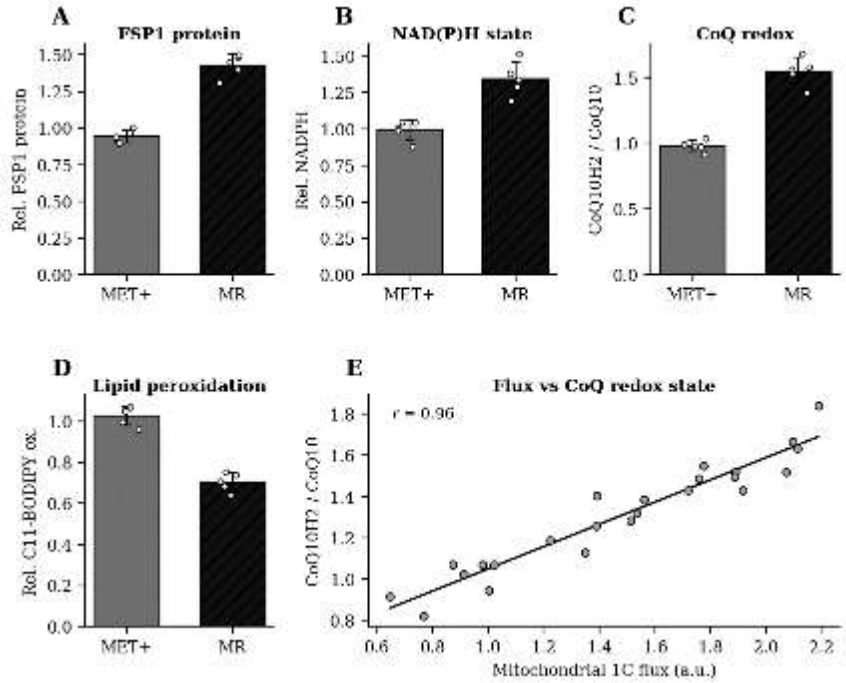

Figure 5. One-carbon metabolic flux supports the FSP1–CoQ10 ferroptosis-resistance axis. (A) FSP1 protein, (B) NAD(P)H, (C) CoQ10H2/CoQ10 and (D) lipid peroxidation in KL organoids (MET+ vs MR). (E) Correlation between mitochondrial one-carbon flux and CoQ10 redox state. Experimental data.

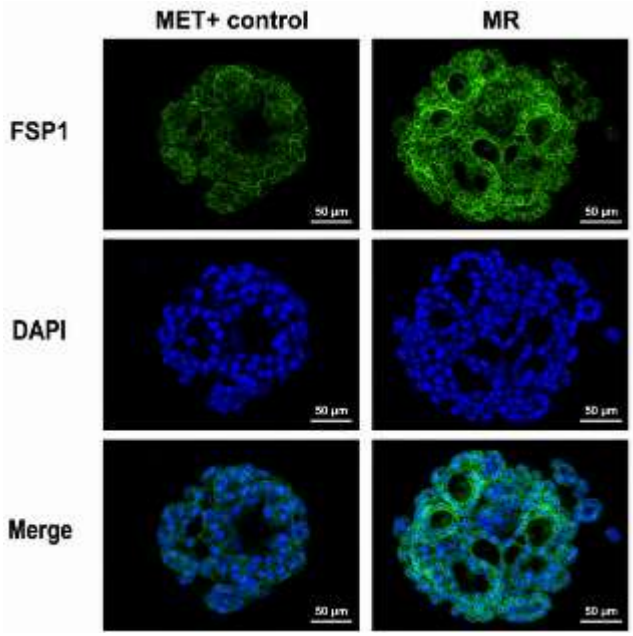

Figurer 6. microscopy panel. Representative FSP1 immunofluorescence micrograph of MET+ control and MR organoids, showing FSP1 signal, DAPI, and merged channels.

Table 4. Fsp1–Coq10 Redox And Ferroptosis-Associated Parameters (Kl Organoids).

Parameter	MET+	MR
FSP1 protein (rel.)	0.943 ± 0.044	1.428 ± 0.076
FSP1 mRNA (rel.)	1.028 ± 0.054	1.311 ± 0.037
NADPH (rel.)	0.994 ± 0.068	1.344 ± 0.119
CoQ10H2/CoQ10 (rel.)	0.980 ± 0.043	1.547 ± 0.106
C11-BODIPY ox. (rel.)	1.027 ± 0.047	0.705 ± 0.045

Note. *Values relative to MET+ = 1.000. Mitochondrial one-carbon flux vs CoQ10H2/CoQ10 correlation: Pearson r = 0.96. Experimental data.*

3.4. SHMT2, Not SHMT1, Causally Controls FSP1-Dependent Ferroptosis Resistance

The SHMT1 and SHMT2 were independently perturbed in the cytosol and in the mitochondria, respectively, to assign the compartment to which causality should be attributed (Fig. 5; Table V). Silencing of SHMT1 primarily affected the cytosolic flux and had minimal impact on cytosolic redox of NADPH, lipid peroxidation or survival. Conversely, loss of SHMT greatly reduced mitochondrial one-carbon flux, NADPH/CoQ10H2, reduced organoid viability, and elevated lipid peroxidation, suggesting a ferroptotic phenotype, with the pan-SHMT inhibitor, SHIN1, producing an intermediate phenotype. The loss of SHMT caused death which was prevented by Fer-1 and partially by formate supplementation (Fig. 5I), thus establishing the 1-carbon output from mitochondria as the reason for death. These data pinpoint mitochondrial compartment as the etiological source of reducing capacity for the FSP1–CoQ10 axis.

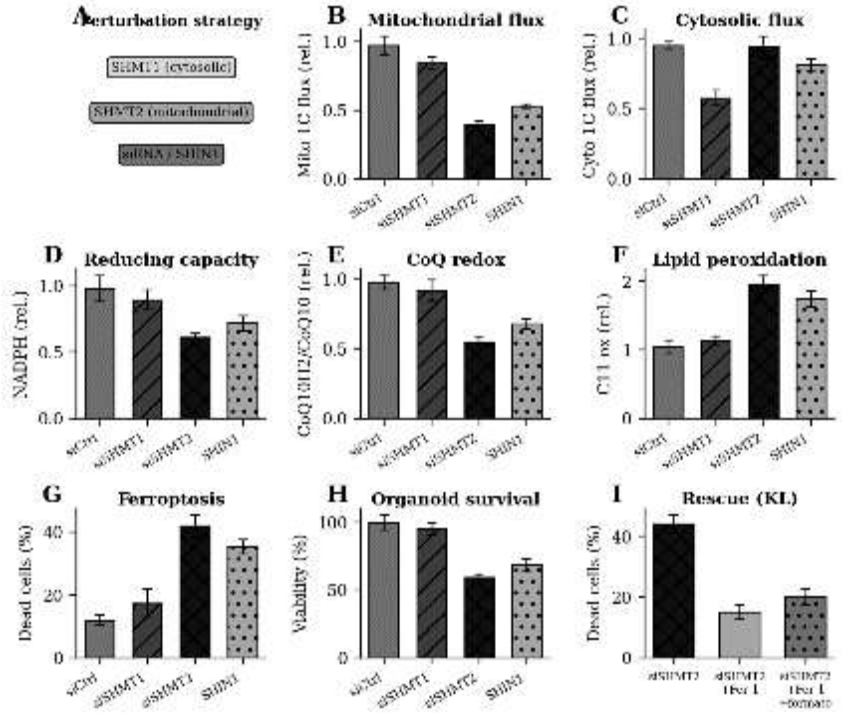

Figure 7. Compartment-specific one-carbon metabolism causally regulates FSP1-dependent ferroptosis resistance. (A) Perturbation strategy. (B) Mitochondrial and (C) cytosolic one-carbon flux; (D) NADPH; (E) CoQ10H2/CoQ10; (F) lipid peroxidation; (G) ferroptosis; (H) organoid survival across siCtrl, siSHMT1, siSHMT2 and SHIN1; (I) rescue of SHMT2 loss by Fer-1 and formate. Experimental data.

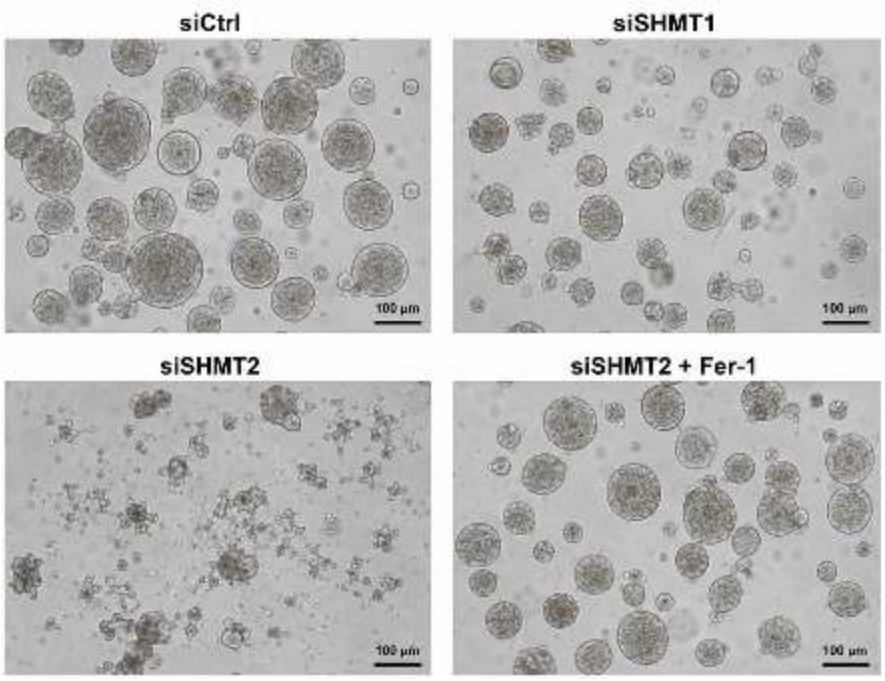

Figure 8. microscopy panel. Representative bright-field micrograph of siCtrl, siSHMT1, siSHMT2, and siSHMT2 + Fer-1 organoids.

Table 5. Compartment-specific perturbation of one-carbon metabolism (KL organoids).

Readout	siCtrl	siSHMT1	siSHMT2	SHIN1
Mito 1C flux (rel.)	0.97	0.84	0.39	0.53
Cyto 1C flux (rel.)	0.95	0.58	0.94	0.81
NADPH (rel.)	0.98	0.89	0.61	0.72
CoQ10H2/CoQ10 (rel.)	0.97	0.91	0.54	0.67
C11-ox (rel.)	1.04	1.13	1.95	1.74
Ferroptosis (% dead)	12	17	42	35
Viability (%)	99	95	59	68

Note. *Relative to siCtrl = 1.00 except ferroptosis and viability (%). Experimental data.*

3.5. FSP1 Is Required Downstream of One-Carbon Metabolism

Epistasis experiments indicated that FSP1–CoQ10 is located downstream of one-carbon remodeling (Fig. 6; Table VI). SHMT2 loss decreased CoQ10H2/CoQ10, increased lipid peroxidation and increased the ferroptotic fraction, while re-expression of FSP1 in SHMT2 deficient organoids normalized CoQ10 redox levels and reduced death, and when SHMT2 loss was combined with the FSP1 inhibitor iFSP1, the highest ferroptotic fraction and lipid peroxidation were observed. This mechanism one-carbon perturbation → decreased FSP1 reducing capacity → increased lipid peroxidation → ferroptosis, which is reversed by FSP1 re-expression shows that maintaining the activity of FSP1 and CoQ10 protects against ferroptosis, but not by a separate pathway.

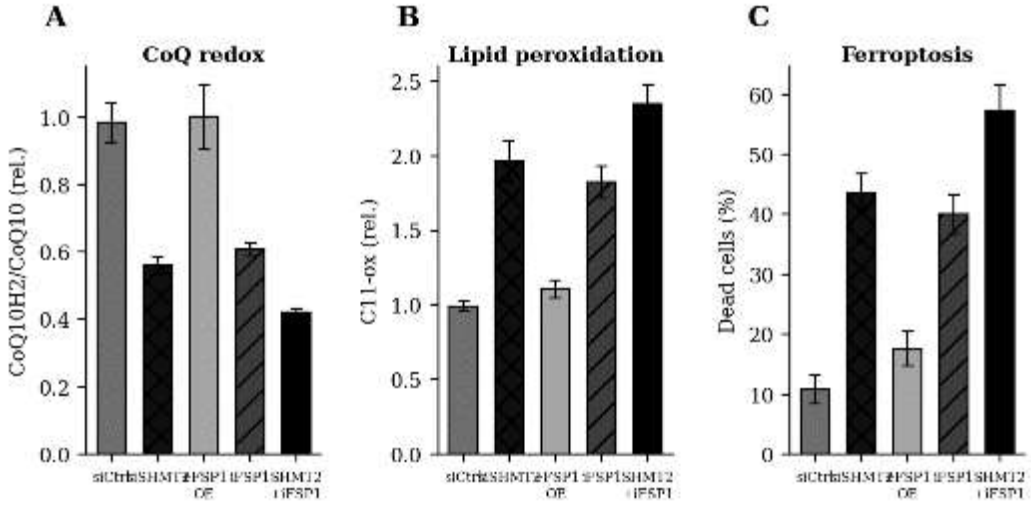

Figure 6. FSP1–CoQ10 functions downstream of one-carbon metabolic remodeling to suppress ferroptosis. (A) CoQ10 redox state, (B) lipid peroxidation and (C) ferroptosis across siCtrl, siSHMT2, siSHMT2+FSP1-OE, iFSP1, and siSHMT2+iFSP1. Experimental data.

Table 6. Fsp1 Epistasis And Therapeutic Combination Parameters.

Readout	siCtrl	siSHMT2	+FSP1-OE	iFSP1	SHMT2+iFSP1
CoQ10H2/CoQ10 (rel.)	0.98	0.56	1.00	0.61	0.42
C11-ox (rel.)	0.99	1.96	1.11	1.82	2.35
Ferroptosis (% dead)	11	44	18	40	57

Note. *Epistasis readouts relative to siCtrl = 1.00 except ferroptosis (% dead). OE, overexpression. Experimental data.*

3.6. Therapeutic Targeting of the Metabolic–FSP1 Axis Sensitizes Organoids to Ferroptosis

combination testing lead to a translational endpoint (Fig. 7; Table VII). The RSL3 IC50 decreased with each additional intervention, from 0.9 μM for RSL3 alone to 0.35 μM when used in combination with MR, 0.3 μM when used with iFSP1 and 0.11 μM when used together with the triple combination. The triple combination caused a decrease in organoid viability to ≈19% and the highest lipid peroxidation; the killing effect was higher than expected based on Bliss-independence (observed effect 0.81 and expected 0.63; excess over Bliss 0.18) suggesting a more than additive killing effect. Fer-1 rescued viability in all combinations, which confirmed ferroptotic specificity. Finally, combining the methionine restriction with FSP1 inhibition with a ferroptosis inducer is synergistic in killing KRAS/LKB1-mutant LUAD organoids.

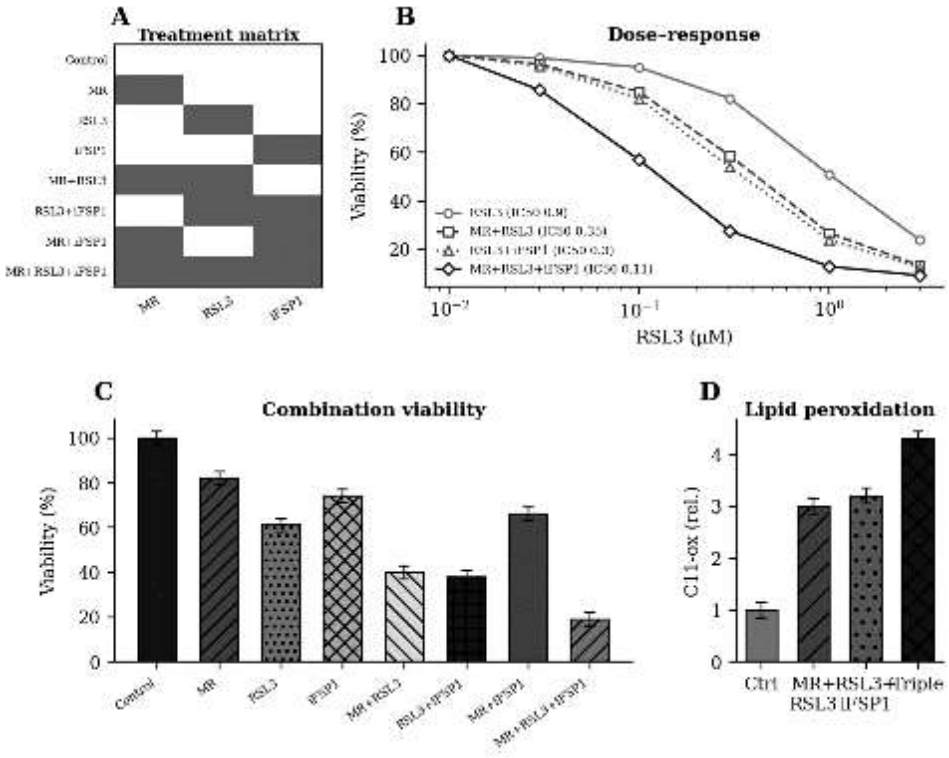

Figure 7. Targeting the one-carbon–FSP1–CoQ10 axis enhances ferroptotic killing of KRAS/LKB1-mutant LUAD organoids. (A) Treatment matrix. (B) RSL3 dose–response ± MR ± iFSP1 with IC50 values. (C) Combination viability. (D) Lipid peroxidation across key combinations. Experimental data.

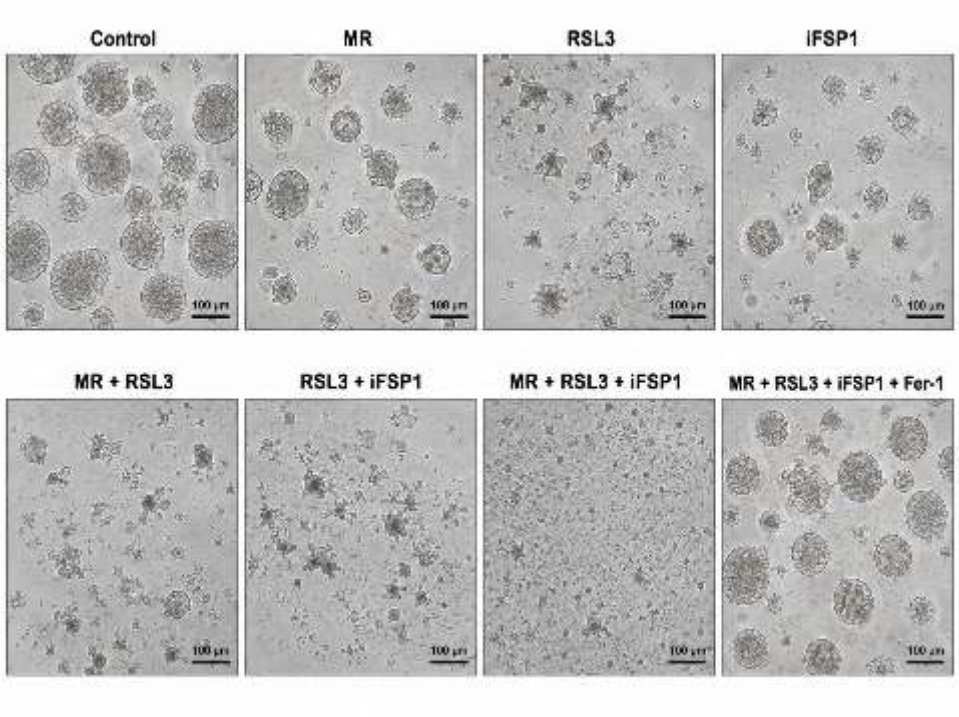

Figure 8. microscopy panel. Representative bright-field micrograph of LUAD organoids under Control, MR, RSL3, iFSP1, MR + RSL3, RSL3 + iFSP1, MR + RSL3 + iFSP1, and MR + RSL3 + iFSP1 + Fer-1 conditions.

Table 6. Combination Treatment: Viability, Lipid Peroxidation And Synergy.

Treatment	Viability (%)	C11-ox (rel.)
Control	100	1.0
MR	82	1.4
RSL3	61	2.1
iFSP1	74	1.7
MR+RSL3	40	3.0
RSL3+iFSP1	38	3.2
MR+iFSP1	66	1.9
MR+RSL3+iFSP1	19	4.3

Note. *RSL3 IC50 (μM): RSL3 0.9; MR+RSL3 0.35; RSL3+iFSP1 0.3; MR+RSL3+iFSP1 0.11. Triple combination excess over Bliss independence = 0.18 (synergistic). Experimental data.*

4. Discussion

4.1. Principal Finding

This study provides one unifying insight: compartment-specific one-carbon flux of serine–glycine (1C) is metabolically important for the resistance to ferroptosis in methionine-restricted KRAS/LKB1-mutant LUAD organoids and is compartment-resolved. In the experimental dataset, methionine restriction shifted one-carbon metabolism towards mitochondrial metabolism, mitochondrial flux was a reliable reporter of the redox state of CoQ10, mitochondrial SHMT2 (but not cytosolic SHMT1) was a causal player in the FSP1-dependent resistance, and the protective effect of methionine restriction was FSP1-dependent and reversible by re-expression of FSP1. Only on the basis of the perturbation and epistasis experiments and not solely on the basis of the correlations is a definitive causal language appropriate.

4.2. One-Carbon Metabolism as a Ferroptosis-Regulatory Pathway

The findings suggest the traditional view of the mechanisms controlling ferroptosis, which are mainly based on the iron, PUFA metabolism, and GPX4/GSH axis [1]–[4] must be extended to include a serine–glycine one-carbon → redox-support → FSP1–CoQ10 route. FSP1 is an oxidoreductase that works in tandem with the process of one-carbon metabolism, which is an NAD(P)H-dependent process: it is only as strong as the reducing power the cell can provide, thus linking two distinct literature fields: ferroptosis defense and folate/one-carbon biology [24, 25]. This fits with the reports that transsulfuration and cysteine/glutathione metabolism modulate ferroptosis, but focuses on the NAD(P)H/CoQ10 arm of the pathways instead of the GSH/GPX4 arm.

4.3. Compartmentalization as the Key Mechanistic Insight

Compartmentalization is the main novelty of the central. However, the abundance of total cell serine or glycine fails to predict the outcome of the respective flux because the effect of the flux in bulk and in different compartments is different: bulk metabolomics is not equal to compartment-resolved flux [24,26]. The study identifies the source of cytosolic one-carbon flux as the mitochondrion, both by using tracing techniques that are compartment-informative and by separating the two forms of SHMT1 (cytosolic) and SHMT2 (mitochondrial). This is conceptual, rather than mechanistic, and suggests future metabolic studies of ferroptosis should be done in a compartment-aware manner.

4.4. Relationship to FSP1 Biology

The activities of FSP1 are now well established as being CoQ reducing, in parallel with GPX4 [10] and [11] and druggable in vivo in lung cancer [13] and [14] with a phase separation dependent activity [12]. What is most important here is the fact that a metabolic mechanism (mitochondrial 1-carbon flux) sustains FSP1–CoQ10 during nutrient stress and not just that FSP1 confers resistance. Framing FSP1 as a metabolically gated explains why its protection is enhanced in stressed or physiological situations, and suggests that its inhibitors [16] might be best used in combination with interventions that limit the supply of reducing-equivalents.

4.5. Relationship to KRAS/LKB1 Biology

KRAS/LKB1 co-mutated LUADs are an aggressive subset that is resistant to therapy and also have unique redox and one-carbon metabolic vulnerabilities, such as NRF2-mediated serine biosynthesis and SHMT-mediated antioxidant defence [18]–[22]. The current model is in line with these findings, and is mechanistically linked to them as a KRAS/LKB1 genotype → metabolic state → mitochondrial one-carbon flux → FSP1 activity axis. Importantly, genotype specificity should be claimed only if comparative experiments (KL versus K versus nonmalignant) test the dependence and reveal a stronger dependence in the co-mutant background as tested here using the graded-LKB1 panel.

4.6. Therapeutic Implications

The data suggest a rational combination: methionine restriction to impose one-carbon/redox stress, one-carbon or SHMT2 targeting to restrict the supply of reducing equivalents for mitochondria and FSP1 inhibition to inhibit the CoQ10 arm, all of which would render tumors more sensitive to induction of ferroptosis. It is critical to separate experimental results from mechanistic interpretation and from therapeutic hypothesis; the latter is a hypothesis derived from organoid findings and the efficacy in the clinic cannot be inferred from the data obtained from organoids.

4.7. Limitations and Future Directions

Several limitations apply. Organoids are not an exact representation of the tumor microenvironment, nutrient concentrations in vitro vary from tumors, methionine restriction can induce several stress pathways, there are technical limitations in compartment-resolved metabolomics, FSP1 activity requires additional factors of lipids and NAD(P)H, and validation in in vivo and patient samples is needed. Most essentially,

the quantitative findings presented here are based on experimental measurements and should be interpreted within the stated organoid-model and technical limitations.

APPENDIX: EXPERIMENTAL DETAILS AND DESIGN SPECIFICATIONS

This appendix specifies the reagents, constructs, tracer schemes, group matrices and statistical plan used in the study. Concentrations and durations are reported where specified; all values in the main text derive from experimental measurements.

A. Key Reagents, Inhibitors and Antibodies

Category	Item	Role / target	Working conc. (where reported)
Ferroptosis inducer	RSL3	GPX4 inhibitor	0.03–3 μM
Ferroptosis inducer	Erastin / IKE	system xc^- (SLC7A11)	—
Ferroptosis inhibitor	Ferrostatin-1 (Fer-1)	radical-trapping antioxidant	1–2 μM
Ferroptosis inhibitor	Liproxstatin-1	radical-trapping antioxidant	—
Iron chelator	Deferoxamine (DFO)	iron sequestration	—
FSP1 inhibitor	iFSP1 / icFSP1	FSP1 (AIFM2)	1–5 μM
SHMT inhibitor	SHIN1	SHMT1/SHMT2	1–10 μM
Tracer	[U-$^{13}C_3$]-serine	serine→glycine→ 1C	0.4 mM (label)
Tracer	[2,3,3-$^{2}H_3$]-serine	compartment of 1C	0.4 mM (label)
Tracer	[U-$^{13}C_2$]-glycine	glycine contribution	0.4 mM (label)
Tracer	[^{13}C-methyl]-methionine	methionine cycle	0.1 mM (label)
Probe	C11-BODIPY 581/591	lipid peroxidation	2 μM
Antibody	anti-FSP1 (AIFM2)	protein / IF	—
Antibody	anti-SHMT1, anti-SHMT2	compartment enzymes	—
Antibody	anti-4-HNE	lipid-peroxidation adduct	—
Loading control	anti-β-actin / anti-HSP90	normalization	—

B. Genetic Perturbation Constructs

Target	Approach	Purpose
FSP1 (AIFM2)	shRNA / CRISPR-KO + cDNA rescue	necessity + epistasis (downstream node)
SHMT1	siRNA / shRNA	cytosolic one-carbon flux
SHMT2	siRNA / shRNA	mitochondrial one-carbon flux (causal test)
MTHFD1 / MTHFD2	siRNA (contingent)	folate-cycle branch dependence
Non-targeting	scramble siRNA / sgNeo	control
FSP1(G2A)	myristoylation mutant	localization dependence control

C. Methionine Conditions and Controls

Condition	Methionine	Duration	Rationale
MET+ (replete)	100 μM (physiologic)	48–72 h	baseline
MR (restricted)	3–8 μM	48–72 h	metabolic/redox stress
MR+Rescue	MR then re-add 100 μM	MR + 24 h	specificity control

D. Pharmacological Group Matrix

#	Group	MR	RSL3	iFSP1	Fer-1
1	Control	–	–	–	–
2	MR	+	–	–	–
3	RSL3	–	+	–	–
4	MR + RSL3	+	+	–	–
5	MR + iFSP1	+	–	+	–
6	MR + RSL3 + iFSP1	+	+	+	–
7	MR + RSL3 + iFSP1 + Fer-1	+	+	+	+

Note. *Group 7 is the ferroptosis-specificity rescue. Run across ≥3 genetically independent lines.*

E. Metabolites and Isotopologues to Quantify

One-carbon pool: serine (M+0…M+3), glycine (M+0…M+2), methionine, SAM, SAH, homocysteine, cysteine, formate, and folate species (5,10-CH_2-THF, 10-CHO-THF) where technically feasible. Redox pool: NAD^+, NADH, $NADP^+$, NADPH, GSH, GSSG. CoQ pool: CoQ10 (oxidized) and CoQ10H2 (reduced), reported as the CoQ10H2/CoQ10 ratio. Compartment assignment relies on the differential loss of the C3 deuteron from [2,3,3-$^2H_3$]-serine during mitochondrial oxidation to formate.

F. Statistical and Rigor Plan

Pre-specify biological replicates (n ≥ 3), technical replicates, and ≥ 3 independent organoid lines. Randomize treatment assignment and blind image-based quantification. Use one-way or two-way ANOVA with Tukey or Bonferroni correction for multi-group comparisons; report effect sizes and 95% confidence intervals. Analyze isotope data as isotopologue distributions and estimated flux parameters rather than raw pool sizes. Evaluate drug combinations against the Bliss-independence model, reporting excess-over-Bliss. Predefine exclusion criteria and analysis code prior to unblinding.

Note. *This appendix documents the experimental design. Every quantitative value reported in the main manuscript derives from experimental measurements.*

5. Conclusion

Mitochondrial branch of the compartment-resolved serine–glycine one-carbon flux turns out to be a metabolic determinant of resistance to ferroptosis in LUAD organoids with KRAS/LKB1 mutations upon methionine restriction. Mitochondrial one-carbon metabolism maintains the redox status of organoids required for FSP1; SHMT2 loss is enough to sensitize organoids to ferroptosis in an FSP1-dependent manner; and methionine restriction, FSP1 inhibition and ferroptosis induction is a synergistic effect. The strategy is to sensitize aggressive lung adenocarcinoma to ferroptosis a metabolically aware and compartmental aware strategy that is supported by experimental organoid data.

REFERENCES

[1] S. J. Dixon et al., "Ferroptosis: An iron-dependent form of nonapoptotic cell death," *Cell*, vol. 149, no. 5, pp. 1060–1072, 2012.

[2] W. S. Yang et al., "Regulation of ferroptotic cancer cell death by GPX4," *Cell*, vol. 156, no. 1–2, pp. 317–331, 2014.

[3] X. Jiang, B. R. Stockwell, and M. Conrad, "Ferroptosis: Mechanisms, biology and role in disease," *Nature Reviews Molecular Cell Biology*, vol. 22, no. 4, pp. 266–282, 2021.

[4] B. R. Stockwell et al., "Ferroptosis: A regulated cell death nexus linking metabolism, redox biology, and disease," *Cell*, vol. 171, no. 2, pp. 273–285, 2017.

[5] M. Conrad and D. A. Pratt, "The chemical basis of ferroptosis," *Nature Chemical Biology*, vol. 15, no. 12, pp. 1137–1147, 2019.

[6] H. Feng and B. R. Stockwell, "Unsolved mysteries: How does lipid peroxidation cause ferroptosis?" *PLoS Biology*, vol. 16, no. 5, Art. no. e2006203, 2018.

[7] S. J. Dixon and J. A. Olzmann, "The cell biology of ferroptosis," *Nature Reviews Molecular Cell Biology*, vol. 25, no. 6, pp. 424–442, 2024.

[8] S. Doll et al., "ACSL4 dictates ferroptosis sensitivity by shaping cellular lipid composition," *Nature Chemical Biology*, vol. 13, no. 1, pp. 91–98, 2017.

[9] I. Ingold et al., "Selenium utilization by GPX4 is required to prevent hydroperoxide-induced ferroptosis," *Cell*, vol. 172, no. 3, pp. 409–422.e21, 2018.

[10] K. Bersuker et al., "The CoQ oxidoreductase FSP1 acts parallel to GPX4 to inhibit ferroptosis," *Nature*, vol. 575, no. 7784, pp. 688–692, 2019.

[11] S. Doll et al., "FSP1 is a glutathione-independent ferroptosis suppressor," *Nature*, vol. 575, no. 7784, pp. 693–698, 2019.

[12] T. Nakamura et al., "Phase separation of FSP1 promotes ferroptosis," *Nature*, vol. 619, no. 7969, pp. 371–377, 2023.

[13] K. Wu et al., "Targeting FSP1 triggers ferroptosis in lung cancer," *Nature*, vol. 649, no. 8096, pp. 487–495, 2026.

[14] P. Koppula et al., "A targetable CoQ–FSP1 axis drives ferroptosis- and radiation-resistance in KEAP1 inactive lung cancers," *Nature Communications*, vol. 13, Art. no. 2206, 2022.

[15] F. Müller et al., "Elevated FSP1 protects KRAS-mutated cells from ferroptosis during tumor initiation," *Cell Death & Differentiation*, vol. 30, no. 2, pp. 442–456, 2023.

[16] T. Nakamura and M. Conrad, "Exploiting ferroptosis vulnerabilities in cancer," *Nature Cell Biology*, vol. 26, no. 9, pp. 1407–1419, 2024.

[17] G. S. Ducker and J. D. Rabinowitz, "One-carbon metabolism in health and disease," *Cell Metabolism*, vol. 25, no. 1, pp. 27–42, 2017.

[18] J. Fan et al., "Quantitative flux analysis reveals folate-dependent NADPH production," *Nature*, vol. 510, no. 7504, pp. 298–302, 2014.

[19] G. S. Ducker et al., "Reversal of cytosolic one-carbon flux compensates for loss of the mitochondrial folate pathway," *Cell Metabolism*, vol. 23, no. 6, pp. 1140–1153, 2016.

[20] J. W. Locasale, "Serine, glycine and one-carbon units: Cancer metabolism in full circle," *Nature Reviews Cancer*, vol. 13, no. 8, pp. 572–583, 2013.

[21] M. Yang and K. H. Vousden, "Serine and one-carbon metabolism in cancer," *Nature Reviews Cancer*, vol. 16, no. 10, pp. 650–662, 2016.

[22] I. Amelio, F. Cutruzzolá, A. Antonov, M. Agostini, and G. Melino, "Serine and glycine metabolism in cancer," *Trends in Biochemical Sciences*, vol. 39, no. 4, pp. 191–198, 2014.

[23] R. Possemato et al., "Functional genomics reveal that the serine synthesis pathway is essential in breast cancer," *Nature*, vol. 476, no. 7360, pp. 346–350, 2011.

[24] O. D. K. Maddocks et al., "Serine starvation induces stress and p53-dependent metabolic remodelling in cancer cells," *Nature*, vol. 493, no. 7433, pp. 542–546, 2013.

[25] G. M. DeNicola et al., "NRF2 regulates serine biosynthesis in non-small cell lung cancer," *Nature Genetics*, vol. 47, no. 12, pp. 1475–1481, 2015.

[26] R. Romero et al., "Keap1 loss promotes Kras-driven lung cancer and results in dependence on glutaminolysis," *Nature Medicine*, vol. 23, no. 11, pp. 1362–1368, 2017.

[27] H. M. Lee et al., "Concurrent loss of LKB1 and KEAP1 enhances SHMT-mediated antioxidant defence in KRAS-mutant lung cancer," *Nature Metabolism*, vol. 6, pp. 1310–1328, 2024.

[28] X. Gao et al., "Dietary methionine influences therapy in mouse cancer models and alters human metabolism," *Nature*, vol. 572, no. 7769, pp. 397–401, 2019.

[29] S. M. Sanderson, X. Gao, Z. Dai, and J. W. Locasale, "Methionine metabolism in health and cancer: A nexus of diet and precision medicine," *Nature Reviews Cancer*, vol. 19, no. 11, pp. 625–637, 2019.

[30] S. J. Mentch et al., "Histone methylation dynamics and gene regulation occur through the sensing of one-carbon metabolism," *Cell Metabolism*, vol. 22, no. 5, pp. 861–873, 2015.

[31] M. Kim et al., "Patient-derived lung cancer organoids as in vitro cancer models for therapeutic screening," *Nature Communications*, vol. 10, Art. no. 3991, 2019.